Korean J. Chem. Eng., 37(12), 2152-2160 (2020)
DOI: 10.1007/s11814-020-0635-x

pISSN: 0256-1115
eISSN: 1975-7220

Improvement of low-temperature NH_3-SCR catalytic activity over Mn-Ce oxide catalysts supported on sewage sludge char activated with KOH and H_3PO_4

Junchao Xu*,,†, Xiangyang Zhang*, Yunlan Sun***, Hongming Long*,†, and Zhimin Zheng***

*Key Laboratory of Metallurgical Emission Reduction & Resources Recycling (Anhui University of Technology), Ministry of Education, 243002 Maanshan, P. R. China
**Key Laboratory of Energy Thermal Conversion and Control of Ministry of Education, Southeast University, Nanjing 210096, Jiangsu Province, P. R. China
***School of Petroleum Engineering, Changzhou University, Changzhou 213164, Jiangsu Province, P. R. China
(*Received 25 April 2020 • Revised 1 July 2020 • Accepted 11 July 2020*)

Abstract−Pyrolysis is a very potential sludge treatment technology that is low-cost and environmentally friendly; particularly, the pyrolysis sewage sludge char (SC) can be used as a catalyst support. To improve the NO conversion efficiency of sludge char based catalysts, they were activated by potassium hydroxide and phosphoric acid, respectively. The catalysts of activated sludge char with or without Mn-Ce impregnation in the application of NO removal by low-temperature SCR were investigated. The higher NO conversion efficiency of sludge char based Mn-Ce catalysts at low temperature were obtained. Compared with the 59% NO conversion efficiency of Mn-Ce/SC catalyst, the conversion efficiency of catalyst supported on KOH activated char (SCK) achieved 89% at 220 °C and of catalyst supported on H_3PO_4 activated char (SCP) reached 87% at 240 °C. The catalysts were analytically characterized using N_2 adsorption-desorption, XRD, FTIR, NH_3-TPD and XPS measurements. The higher specific area, excellent dispersion of Mn-CeOx and more Brønsted acid sites are responsible for the higher NO conversion efficiency of Mn-Ce/SCK, while the higher NO conversion efficiency of Mn-Ce/SCP is enhanced by more Brønsted acid sites, oxygen-containing and some unique phosphorus-containing oxygen functional groups. It indicates that sludge char activated by KOH and H_3PO_4 is a potential low-temperature catalyst support.

Keywords: Low-temperature, SCR, Sludge Char, Mn-Ce Catalyst, Chemical Activation

INTRODUCTION

Nitrogen oxides (NOx) are one of the main pollutants emitted from fossil fuel combustion. They are highly irritating to the human respiratory tract and cause environmental problems such as smog, acid rain, greenhouse effects and photochemical smog [1-3]. Currently, selective catalytic reduction (SCR) technology is the most effective method to remove NOx, and $WO_3(MoO_3)$-V_2O_5/TiO_2 is the most popular SCR catalyst for industrial applications [4,5], which has been widely used because of its high NO conversion and strong catalytic performance. However, as is known, the activation temperature of this catalyst is very high and it exhibits narrow activity temperature window in the range of 300-400 °C, which makes its catalytic activity significantly decrease under lower flue gas temperature from the cement, steel and glass industries. In addition, it cannot solve catalyst poisoning because of high temperature sintering and dust. The SCR device can be arranged in low temperature conditions to avoid the above problems. Therefore, there is an urgent need to develop low-temperature SCR catalysts with high activity.

Transition-metal oxides such as Fe [6], Cu [7,8], Mn [9-12], and Cr [13] have been widely studied as the main active substances of SCR deNOx catalysts [14]. Especially, MnOx has been drawn much attention due to its excellent low temperature catalytic performance. However, pure MnOx catalysts generally have small specific surface area and their structure is unstable, which makes them unsuitable for practical applications [15]. Therefore, it is usually supported on a catalyst support to achieve higher performance. Many studies have investigated MnOx/TiO_2 catalysts and the results show that the deNOx efficiency could reach more than 90% at low temperature [16,17]. However, the sulfur and water resistance of MnOx/TiO_2 catalysts is very poor. Moreover, Jin [18] and Sjoerd [19] introduced SO_2 and water into simulated flue gas and found that the SO_2 could produce ammonium sulfate covering the active site of catalyst, which decreased the deNOx efficiency substantially. Fortunately, doping CeOx as auxiliary can improve the catalytic activity and sulfur and water resistance of MnOx catalysts. For example, Chen et al. [13] synthesized Mn-Ce composite oxide catalyst that could achieve 98% deNOx efficiency at 120 °C. This is because the Ce addition can improve the ability of NH_3 adsorption and activation of the catalyst, and promote the SCR reaction [20]. At the same time, the addition of Ce will form new active sites on the catalyst surface. These sites will preferentially adsorb SO_2, thereby avoiding the deactivation of the catalyst and improving the SO_2 resistance of catalyst [21]. In summary, the addition of CeOx in Mn oxide catalysts can improve deNOx efficiency and enhance sulfur and water resistance.

Besides TiO_2, Carbon materials and Al_2O_3 are common supports

†To whom correspondence should be addressed.
E-mail: junchxu@ahut.edu.cn, yaflhm@126.com

for Mn-Ce oxide catalysts [22,23]. The carbon material supports mainly include activated carbon (AC), carbon fiber (ACF), and carbon nanotubes (CNTs). AC has good adsorption capacity and chemical stability and can promote the SCR catalytic reaction [10,24]. ACF loading CeO_2 can achieve 93% deNOx efficiency at 240 °C [25]. CNTs also have excellent catalytic performance [26]. However, it was difficult to widely use it and urgent to find new substitutes due to the complexity of the preparation process and the high cost. Among them, biochar has similar properties to traditional carbon materials, such as large specific surface area, strong adsorption capacity, and good chemical stability. In addition, biochar has low preparation cost and wide source of raw materials. Therefore, biochar is potentially an ideal deNOx catalyst support. The NO conversion of biomass carbon is better than that of coal-based activated carbon [27,28]. Cha et al. [29] first studied low temperature SCR of NO over rice straw and sewage sludge derived char which were activated by different ways and found that co-activation char could highly improve deNOx efficiency, demonstrating that biochar is a feasible catalyst support. Yong et al. [30] believe that sludge charcoal has better deNOx performance than ordinary activated carbon. Both Sheng et al. [31] and Singh et al. [32] studied the deNOx performance of MnOx supported on modified cotton stalk pyrolytic carbon. The former made a comparative study of modified cotton biochar and activated carbon based catalysts. They showed that cotton stalk pyrolytic carbon had higher specific surface area and more functional groups than industrial activated carbon, which causes a higher deNOx efficiency. The latter pointed out that the successful development of this catalyst would greatly reduce the cost and have broad market application prospects. Si et al. [33] carried out a comparative test of sulfur resistance of corn straws pyrolysis carbon and coal-based activated carbon loaded with MnOx, and the results showed that the sulfur resistance of catalyst loaded on corn straws pyrolysis carbon was better than that of coal-based activated carbon. To enhance the deNOx performance of the biomass charcoal-supported catalyst, Li et al. [34] used urea to modify the sargassum pyrolysis carbon and obtained higher deNOx efficiency and wider temperature window. On one hand, biochar is one of the most promising support of low temperature SCR catalyst; on the other hand, catalyst of Mn-Ce oxides supported by biochar can achieve good catalytic effects.

Nowadays, sewage sludge is generally treated by burning, landfilling, and other methods after dehydration. Not only does it require high governance costs, but it also causes secondary pollution to the environment. In this study, dry sludge was used as raw material, which was pyrolyzed to obtain sludge biomass char, and then activated with two different reagents, KOH and H_3PO_4, respectively. Finally, Mn-Ce oxide was impregnated on different sludge biochar to prepare catalysts named Mn-Ce/SC, Mn-Ce/SCK, and Mn-Ce/SCP, respectively. The De-NOx activity of these catalysts was studied. The catalysts were characterized by N_2 adsorption-desorption, X-ray fluorescence, XRD, NH_3-TPD, and FTIR.

EXPERIMENTAL

1. Catalyst Preparation

The sewage sludge, which was obtained from an urban sewage treatment plant, was dried and sieved with 40-60 mesh. Table 1 shows the chemical components of SC (sludge char). Among them, SiO_2 is the main content and the content of iron, phosphorus, aluminum, calcium, potassium, and magnesium decreases in order. In addition, iron, phosphorus, and aluminum may promote the SCR reaction to some extent [35,36].

Table 1. Chemical components of sewage sludge

Components (wt%)	SiO_2	P_2O_5	Fe_2O_3	Al_2O_3	CaO	K_2O	MgO
	34.78	17.86	16.17	13.54	7.26	3.55	2.94

The dry sludge was pyrolyzed in a tube furnace for 1 h at 800 °C under N_2 flow of 50 ml/min. For KOH activation, the SC was put into KOH aqueous solution, of which the mass ratio of SC and KOH was 1 : 1. The mixture was stirred and mixed at room temperature for 2 h, then put into a tube furnace, heated to 700 °C and maintained 2 h under N_2 atmosphere. Finally, it was washed with hot distilled water to neutrality and dried under room temperature. The sample was named SCK. For H_3PO_4 activation, the SC was put into H_3PO_4 aqueous solution, and the mass ratio of SC and H_3PO_4 was 1.5 : 1. Subsequent operations were the same as KOH activation. The sample was named SCP.

Mn-Ce was supported on SC, SCK, and SCP by impregnation method. The loading amount of Mn was 5 wt% and the molar ratio Mn/Ce was 2 : 1. Activated and inactivated chars were impregnated in aqueous solution of $Mn(NO_3)_2$ and $Ce(NO_3)_3$, then stirred at room temperature for 4 h, and dried in a 105 °C oven for 24 h. Finally, they were calcined in a tube furnace under N_2 atmosphere at 500 °C for 2 h to decompose the precursor.

2. Catalytic Activity

The deNOx activity test was carried in a fixed-bed SCR catalyst activity test platform. The simulated flue gas was a mixture of NO, NH_3, and O_2. N_2 was used as balance gas, of which NO was 400 ppm NH_3 was 400 ppm; O_2 was 5% volume, N_2 as balance gas, and the total gas flow was 130 ml/min. The test temperature ranged from 80-260 °C, and the gas hourly space velocity (GHSV) was 15,000 h^{-1}. The deNOx efficiency of catalyst is expressed by the NO conversion rate, and the calculation formula is as follows. The C_0 represents the inlet NO gas concentration (ppm), and the C represents the outlet NO gas concentration (ppm).

$$\text{NO conversion}\ (\%) = \frac{C_0 - C}{C_0} \times 100\% \quad (1)$$

3. Characterization

3-1. N_2 Adsorption-desorption

The specific surface area and pore size distribution of the catalysts were measured by the ASAP2460 specific surface area and pore size tester of American Micron Instruments. N_2 was used as adsorbent and liquid nitrogen as coolant. The BET (Brunauer-Emmett-Teller) equation was used to calculate the specific surface area and pore diameter of the samples.

3-2. FTIR

FTIR spectra were recorded on a Nicolet 6700 infrared spectrometer with a detection range of 4,000-400 cm^{-1}.

3-3. XRD

The XRD test was performed by the D8ADVANCE X-ray dif-

fractometer of Bruker, Germany. The radiation source was a standard modified Cu target, and the radiation power was 3 KW. The test step size was 0.02/s, and scanning range was 10-80°.

3-4. NH_3-TPD

NH_3-TPD is often used to detect the number of acidic sites on the catalyst, which is an important means for evaluating the performance of a catalyst. The NH_3-TPD test was performed using an AutoChem1II 2920 chemisorbent. We weighed a sample of certain quality and placed it in a U-shaped quartz tube. The temperature was raised from room temperature to 300 °C at 10 °C/min for drying and pretreatment. The air stream (50 mL/min) was purged for 2 h, cooled to 50 °C, and 10% NH_3/He mixed gas (50 mL/min) for 1 h to saturation. After the samples were purged in an He stream for 1 h to remove physically adsorbed NH_3, the temperature was raised to 500 °C with a heating rate of 10 °C/min. Desorbed NH_3 was detected using a thermal conductivity detector (TCD).

3-5. XPS

X-ray photoelectron spectroscopy (XPS) was performed to investigate the surface chemical states of Mn, Ce species in Mn-Ce/SC, Mn-Ce/SCK and Mn-Ce/SCP with Thermo Scientific K-Alpha. The obtained binding energies were referenced to the C1s line at 284.6 eV.

RESULTS AND DISCUSSION

1. Catalyst Activity

Fig. 1 shows the NO conversion of SC, SCK, and SCP at 80-260 °C. The deNOx efficiency of SC, SCK, and SCP increased with increasing the temperature. Both KOH and H_3PO_4 can increase the NO conversion efficiency, and the NO conversion of SCK is much closer to that of SC. At 240 °C, SCK presents the highest NO conversion of 50%.

Fig. 2 shows NO conversion over Mn-Ce/SC, Mn-Ce/SCK, and Mn-Ce/SCP catalysts. The deNOx efficiency increases with the increasing of temperature. The NH_3-SCR activity of Mn-Ce/SCK and Mn-Ce/SCP catalysts is higher than that of Mn-Ce/SC catalyst. Mn-Ce/SCK catalyst reaches the highest NO conversion of 89% at 200 °C, while the highest NO conversion of Mn-Ce/SC and Mn-Ce/SCP catalyst reached 49% and 87% at 240 °C, respectively, indicating that the catalytic performance of activated carbon can be highly improved by KOH or H_3PO_4 activation. When the temperature ranges from 80-220 °C, SCR activity of Mn-Ce/SCK is higher than that of Mn-Ce/SCP. However, when the temperature increases above 220 °C, the NH_3-SCR activity of Mn-Ce/SCK decreases. The temperature corresponding to the highest deNOx efficiency of Mn-Ce/SCK is lower than that of Mn-Ce/SCP and Mn-Ce/SC. Therefore, KOH activation reduces the temperature corresponding to its highest efficiency. Note that the catalytic efficiency of Mn-Ce/SCK at 200 °C is improved compared with the reported data [29]. This

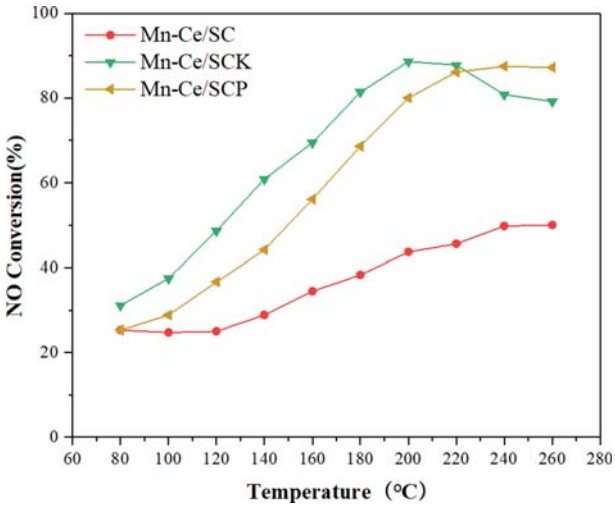

Fig. 2. SCR activity of Mn-Ce/SC, Mn-Ce/SCK and Mn-Ce/SCP at different temperature. Conditions: [NO]=400 ppm, [NH_3]=400 ppm, O_2=5% volume, N_2 balance, GHSV=15,000 h^{-1}.

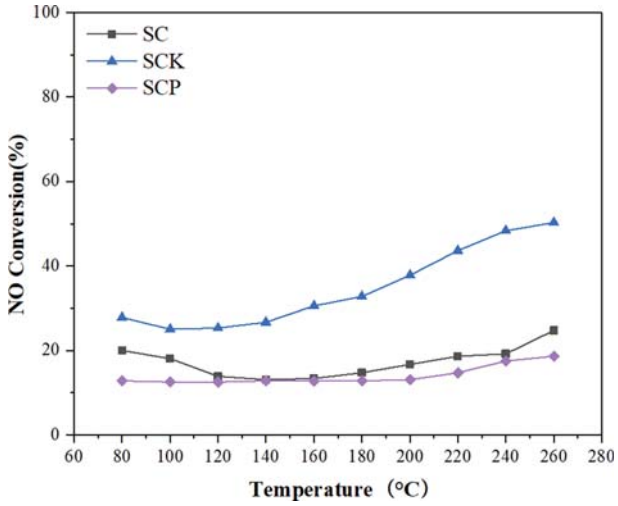

Fig. 1. De-NOx activity of sludge char with or without activation at different temperatures. Conditions: [NO]=400 ppm; [NH_3]=400 ppm; O_2=5% volume; N_2 balance, GHSV=15,000 h^{-1}.

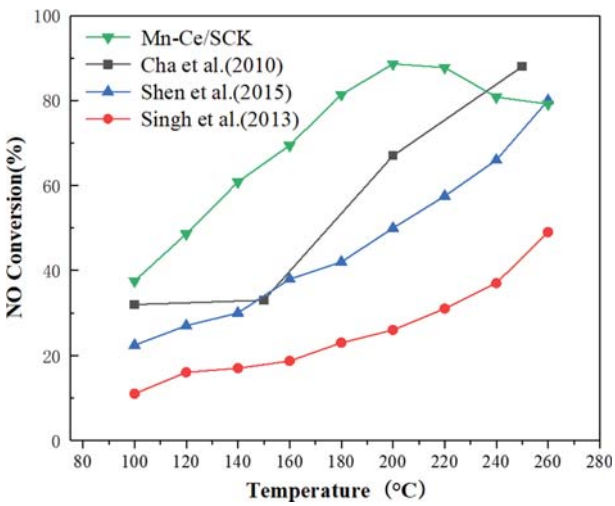

Fig. 3. Activity comparison of Mn-Ce/SCK with other works presented by Cha et al. [29], Shen et al. [31], and Singh et al. [33].

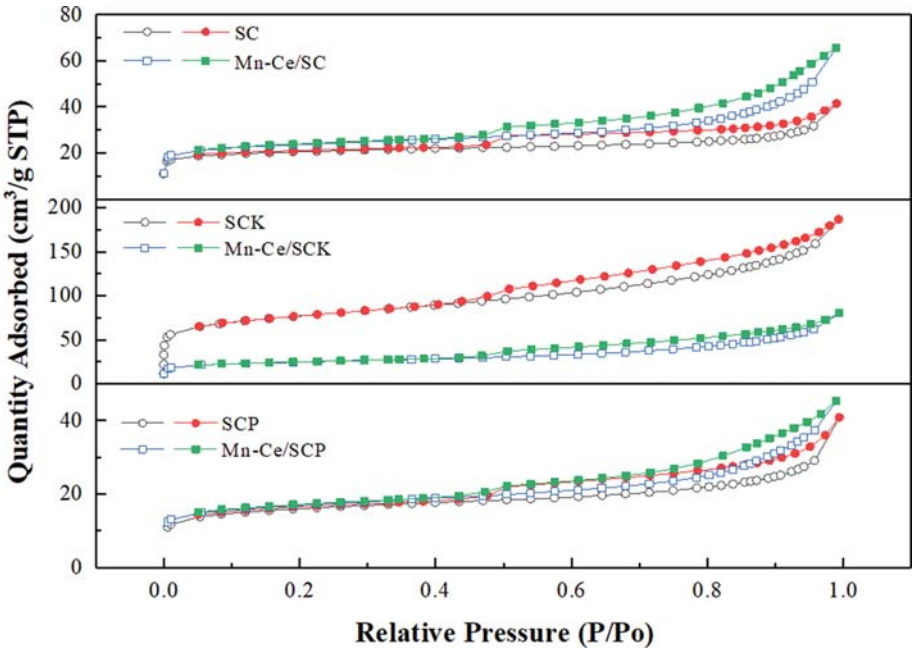

Fig. 4. N_2 adsorption-desorption isotherms of sewage sludge char based catalysts.

is because the addition of CeOx can make NH_3 more easily be adsorbed and activated during the SCR reaction process, and thus the catalytic performance increases [37]. In addition, the order of highest deNOx efficiency of catalysts is SCK>SC≈SCP without Mn-Ce loading, while it changes as Mn-Ce/SCK>Mn-Ce/SCP> Mn-Ce/SC after Mn-Ce loading.

Fig. 3 shows the activity comparison of other similar types of deNOx catalysts with Mn-Ce at 100-220 °C. Compared with previous catalysts, Mn-Ce/SCK has the highest SCR catalytic efficiency.

2. Characterization of Catalysts

2-1. N_2 Adsorption-desorption

The N_2 adsorption and desorption curves of catalysts are shown in Fig. 4. All the curves are convex, and the adsorption amount rises rapidly when the relative pressure is lower than 0.2. When the P/P_0 changes from 0.2 to 0.6, all the curves tend to be stable, and they increase again when the P/P_0 is larger than 0.9. According to the International Union of Pure and Applied Chemistry (IUPAC), the type of these curves is IV adsorption isotherm curve. The internal pore structure is mainly mesoporous. Furthermore, the H4 type hysteresis loop appears in P/P_0 range from 0.4 to 0.6, suggesting that the interior structure of catalysts is mesoporous and the pore type is a slit hole with a layered structure.

Table 2. Physical characteristics of the sewage sludge char based catalysts

Samples	BET surface area (m^2/g)	Pore volume (cm^3/g)	Pore diameter (nm)
SC	64.63	0.039	2.93
SCK	254.57	0.225	3.75
SCP	51.83	0.046	3.33
Mn-Ce/SC	75.54	0.076	4.04
Mn-Ce/SCK	80.64	0.103	4.60
Mn-Ce/SCP	54.63	0.053	4.08

Table 2 shows the specific surface areas, pore volumes, and the pore diameters of different catalysts. After KOH activation, the specific surface area of SCK was significantly increased from 64.63 to 254.57 m^2/g, while the specific surface area of SCP was slightly lower than that of SC after H_3PO_4 activation, which was caused by the reduction of specific surface area of the pores due to the excessive use of phosphoric acid [38]. It can be seen that the surface area of Mn-Ce/SCP is the smallest among them. However, its NOx conversion efficiency is not the worst, indicating that although the surface area of catalyst has effect on the NOx conversions, it is not a decisive factor [39].

As Table 2 shows, the pore diameter of all catalysts increased after Mn-Ce impregnation. It can be explained as follows. The micropores were blocked by Mn-Ce impregnation and formed larger pores. We note that the specific surface areas and the pore volumes of Mn-Ce/SC and Mn-Ce/SCP increase, while those of Mn-Ce/SCK decrease. Fig. 5 shows the pore size distribution obtained by employing the BJH model. More pores at 2-30 nm are observed in Mn-Ce/SCP, while for Mn-Ce/SC catalyst the pores are mainly distributed at 2-100 nm. Therefore, Mn-Ce/SC and Mn-Ce/SCP can form more mesopores after MnOx and CeOx impregnation, which result in the specific surface area becoming larger. Although the Mn-Ce/SCK specific surface area decreases after impregnation, it still has the highest specific surface area among the three catalysts. In summary, chemical activation has a great effect on surface area and pore size distribution, which can facilitate the diffusion of gas and make the reaction occur more easily.

The catalyst specific surface area and NO conversion rate were normalized to further analyze the relationship between them. The results are shown in Table 3; it can be seen that the normalized NO conversion of Mn-Ce/SCP is the highest, indicating that its

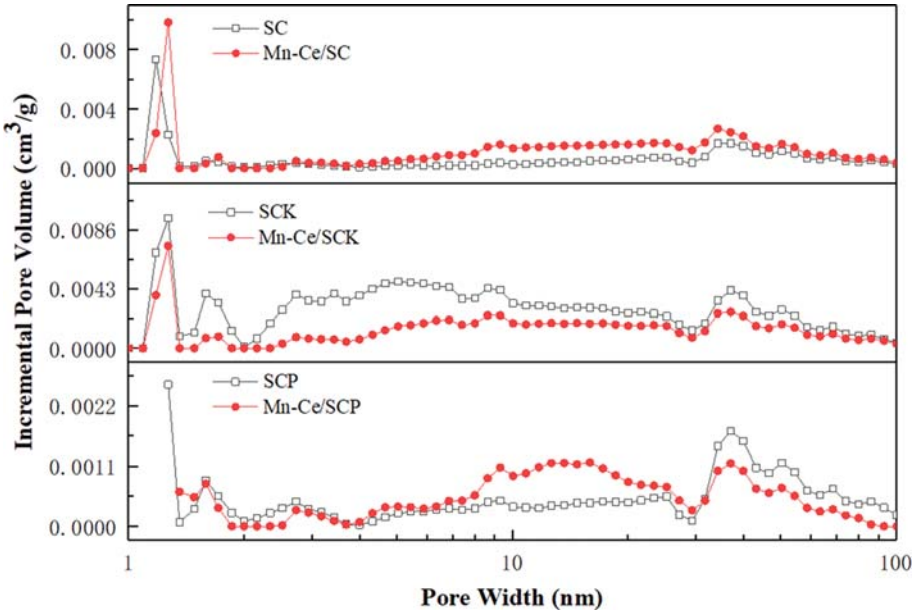

Fig. 5. BJH pore size distribution of sewage sludge char based catalysts.

Table 3. Normalized NO conversion

Catalyst	Value
Mn-Ce/SC	0.66
Mn-Ce/SCK	1.10
Mn-Ce/SCP	1.60

NO conversion efficiency per unit area is higher. Although the NO conversion efficiency per unit area of Mn-Ce/SCK is lower, its high specific surface area makes it show a higher NO conversion rate as a whole.

2-2. FTIR

Fig. 6 shows the FT-IR identification of the functional groups developed on the surface of Mn-Ce/SC, Mn-Ce/SCK, and Mn-Ce/SCP catalysts. The catalysts exhibited broad peaks within the range of 3,500-3,300 cm^{-1}. The absorption peaks of 3,426 cm^{-1} appear due to the O-H bond vibration in the hydroxyl group [40]. The 1,627 cm^{-1} absorption peaks correspond to the vibration of C=O in the carbonyl group. The peaks of 1,386 cm^{-1} correspond to the O-H bond, and 878 cm^{-1} peaks appear due to the C-H out-of-plane bending vibration. The magnitude of the 1,627 cm^{-1} peak was in order of Mn-Ce/SC<Mn-Ce/SCK≈Mn-Ce/SCP, indicating that KOH or H_3PO_4 activation can increase the C=O functional groups. In particular, peaks at 1,465 cm^{-1} (C=C) were observed for Mn-Ce/SC and Mn-Ce/SCK but not for Mn-Ce/SCP. And the intensity of Mn-Ce/SCK was stronger than that of Mn-Ce/SC. Furthermore, Mn-Ce/SCP presents a unique peak of 1,080 cm^{-1} corresponding to P=O due to phosphoric acid activation [29]. Overall, Mn-Ce/SCK and Mn-Ce/SCP have stronger absorption peaks than Mn-Ce/SC, indicating that they have more oxygen-containing functional groups. The oxygen functional groups on the surface of the catalyst are in favor of oxygen transfer during the SCR reaction, thus facilitating the SCR deNOx activity. This is another reason why Mn-Ce/SCK shows the highest SCR deNOx activity. Moreover, due to the rich functional groups, although Mn-Ce/SCP has the lowest specific surface area among the three catalysts, it has high NO conversion as much as Mn-Ce/SCK.

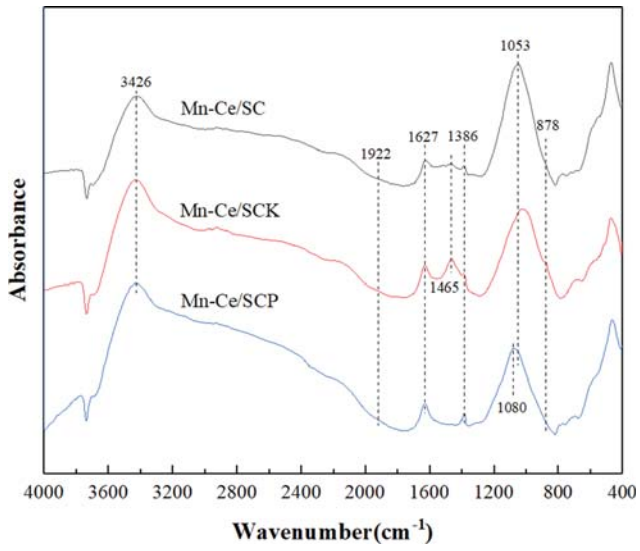

Fig. 6. FTIR spectra of sewage sludge char based catalysts.

2-3. XRD

The XRD patterns of Mn-Ce/SC, Mn-Ce/SCK, and Mn-Ce/SCP are shown in Fig. 7. The wide diffraction peaks of the three samples at around 27° are the characteristic peaks of carbon. Mn-Ce/SC and Mn-Ce/SCP have similar peak distribution. Both of them show obvious diffraction peaks at 21°, 26.6°, and 50.1°, which is considered as SiO_2. However, these peaks do not appear in Mn-Ce/SCK, indicating that the activation of KOH can make SiO_2 transfer to amorphous structure, but the lattice structure of SiO_2 does not have substantial effect on active sites [22]. No diffraction peak corresponding to cerium oxide is found in the three samples,

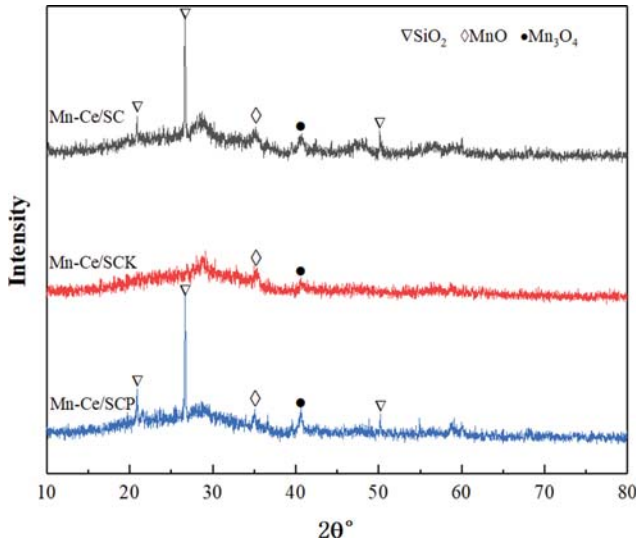

Fig. 7. XRD patterns of sewage sludge char based catalysts.

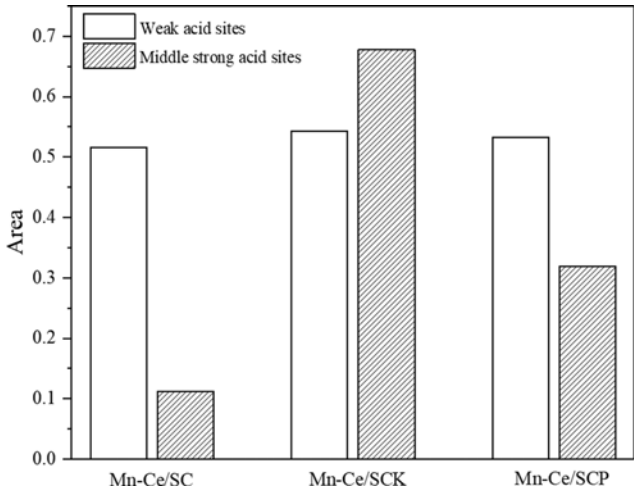

Fig. 9. Acid sites distribution of sewage sludge char based catalysts.

which indicates that it was dispersed on the surface sufficiently. The peaks of 35° and 40.6° correspond to MnO and Mn_3O_4, respectively, and the intensity of the diffraction peaks of MnO and Mn_3O_4 in Mn-Ce/SCK is lower than that of Mn-Ce/SC and Mn-Ce/SCP, indicating that manganese oxide has excellent dispersion on the surface of Mn-Ce/SCK, which is probably another reason that Mn-Ce/SCK exhibits the highest catalytic performance compared to the other two catalysts.

2-4. NH_3-TPD

Fig. 8 shows the NH_3-TPD curves of the Mn-Ce/SC, Mn-Ce/SCK, and Mn-Ce/SCP catalysts. Generally, the peaks at 100-150 °C and 350-440 °C are considered weak acid site distributions [23] and a medium-strong acid [41] corresponding to the distribution of Brønsted acid sites. It can be seen that the three catalysts have weak acid sites and Brønsted acid sites, but the number of Brønsted acid sites is not the same in different catalysts [42]. Overall, the amount of surface acidity increases in the order of Mn-Ce/SCK> n-Ce/SCP>Mn-Ce/SC. Because the adsorption and activation of NH_3 on the acid sites of the catalyst surface are key steps, the more acid sites, the easier adsorption and activation of NH_3. Therefore, more acid sites can promote the improvement of NO conversion. This is the reason why Mn-Ce/SCK shows the highest deNOx efficiency.

Fig. 9 shows the corresponding number of two acid sites in the three catalysts. The same kinds of acid sites are found in the three catalysts. According to the literature [43], the middle strong acid in this type of catalyst can be considered as the Brønsted acid site. After chemical activation, the number of weak acid sites hardly changes, whereas the number of Brønsted acid sites is in the order of Mn-Ce/SCK>Mn-Ce/SCP>Mn-Ce/SC, and it is consistent with the highest deNOx efficiency of the catalysts. Therefore, it suggests that chemical activation can increase the number of Brønsted acid sites for the sewage sludge. As we known, the adsorption and activation of NH_3 are important steps in deNOx reaction, and more acid sites facilitate the adsorption of NH_3 and the reaction. How-

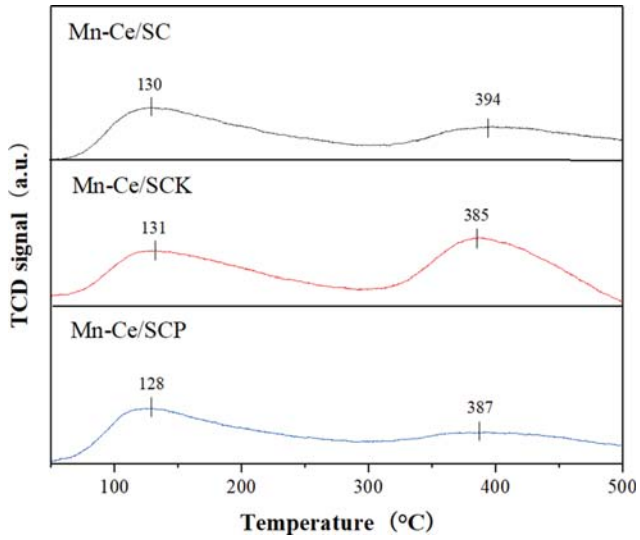

Fig. 8. NH_3-TPD profiles of sewage sludge char based catalysts.

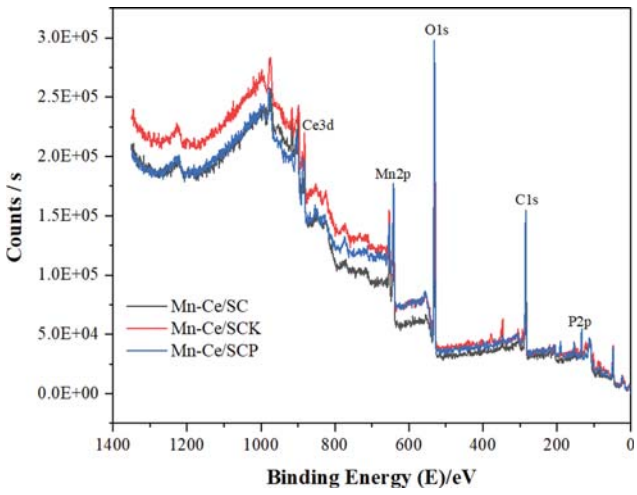

Fig. 10. The XPS survey spectrum of Mn-Ce/SC, Mn-Ce/SCK, and Mn-Ce/SCP.

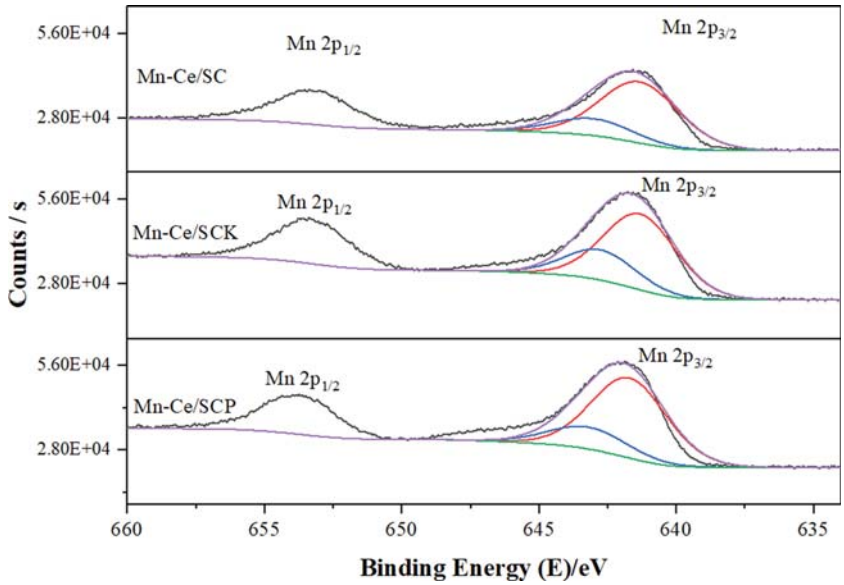

Fig. 11. The XPS spectra of Mn-Ce/SC, Mn-Ce/SCK and Mn-Ce/SCP (Mn 2p).

ever, there are different opinions on which Lewis acid site or Bronsted acid site is more important for the adsorption and activation of NH_3 [43,44]. According to the corresponding results of the above Bronsted acid site and SCR activity, it can be concluded that Brønsted acid sites may play an important role in SCR deNOx catalysts based SC.

2-5. XPS

To determine the chemical states and the form of manganese or cerium species in the catalysts, the Mn-Ce/SC, Mn-Ce/SCK and Mn-Ce/SCP catalysts were examined by XPS. The survey spectrum of the three catalysts is shown in Fig. 10. The XPS peaks of Mn-Ce/SC and Mn-Ce/SCK corresponding to manganese, cerium, carbon and oxygen can be detected. In addition, the survey spectrum of Mn-Ce/SCP can find the phosphorus, because the catalyst is activated by phosphoric acid.

The Mn 2p spectra of the catalysts are presented in Fig. 11, which contained two main peaks at around 641.2 eV and 653.0 eV, assigned to Mn $2p_{3/2}$ and Mn $2p_{1/2}$, respectively. According to the literature [47], the Mn $2p_{3/2}$ peaks of the three catalysts can be well fitted into two characteristic peaks near the 643.5 and 641.2 eV, corresponding to Mn^{4+} and Mn^{3+}, respectively. It shows that the MnOx on the surface of the catalyst coexists in the oxidation states of Mn^{4+} and Mn^{3+}. The relative atomic ratios of Mn^{4+}/Mn^{n+} and Mn^{3+}/Mn^{n+} on the catalysts surface, which are calculated from the

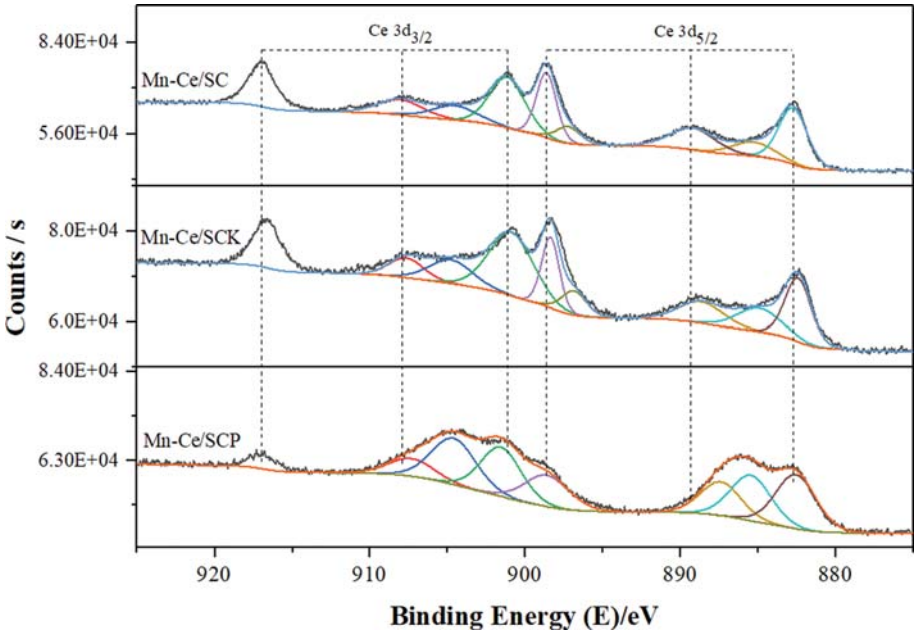

Fig. 12. The XPS spectra of Mn-Ce/SC, Mn-Ce/SCK and Mn-Ce/SCP (Ce 3d).

Table 4. The elemental distribution percentage of the catalyst

Catalyst	Mn^{3+}	Mn^{4+}	Ce^{3+}	Ce^{4+}
Mn-Ce/SC	78.28%	21.72%	15.38%	84.62%
Mn-Ce/SCK	71.98%	28.02%	20.49%	79.51%
Mn-Ce/SCP	77.81%	22.19%	33.6%	66.4%

relative areas of the characteristic peaks, are listed in Table 4. It can be seen that chemical activation enhances the content of Mn^{4+}, and the Mn^{4+} of Mn-Ce/SCK is higher than that of Mn-Ce/SCP. Many studies have shown that higher valence Mn could improve the low temperature deNOx performance of catalysts [46]. Therefore, higher Mn^{4+} content is one of the reasons why Mn-Ce/SCK shows excellent NO conversion at low temperature.

Fig. 12 shows the XPS spectra of Ce 3d, which is a combination of Ce $3d_{3/2}$ and Ce $3d_{5/2}$ spectra. The peaks at 886.00 and 904.6 eV are assigned to Ce^{3+}, while the others are attributed to Ce^{4+} species. Table 4 also displays the ratio of Ce^{3+}/Ce^{n+} and Ce^{4+}/Ce^{n+} calculated based on the fitted area. The result implies that Ce^{4+} is mainly Ce element in all catalysts. The ratio of Ce^{3+} increases from 15.38% of Mn-Ce/SC to 20.49% of Mn-Ce/SCK and 33.6% of Mn-Ce/SCP after chemical activation, which is beneficial to the formation of oxygen vacancies and thus promotes the SCR reaction [48].

SO_2 TOLERANCE

The effect of SO_2 on deNOx efficiency of the three catalysts is shown in Fig. 13. The temperature of the simulated flue gas is 220 °C and the amount of SO_2 addition is 100 ppm. It can be found that the NO conversion curves of the three catalysts show similar trends after the introduction of SO_2. Upon the addition of SO_2 into the simulated gas, the deNOx activity decreases sharply and reaches a steady-state NO conversion of about 29%, 27%, and 6% for Mn-Ce/SCK, Mn-Ce/SCP and Mn-Ce/SC catalysts in about 1 h, respectively. Also, both the H_3PO_4 and KOH activation can slightly improve the SO_2 resistance of catalysts. The main reason for the decrease in catalyst activity is that the ammonium sulfate generated on the catalyst surface covers the acid sites, which hinders the adsorption and activation of NH_3. Although, the acid sites formed by the addition of CeOx can preferentially adsorb SO_2 [21] and protect the acid sites formed by MnOx. However, when the acid sites provided by CeO_2 are exhausted, there are still more SO_2 that reduce the performance of the catalyst inevitably. For this reason, all the three samples show a poor sulfur resistance. After turning off SO_2, the deNOx activity cannot recover. There are two main reasons for the decline in NO conversion efficiency. On one hand, the active site formed by Mn-Ce oxide reacts with SO_2. On the other hand, the ammonium sulfate salt formed by SO_2 and NH_3 covers the surface of the catalyst, which will reduce the exposure of acidic sites and prevent the adsorption of NH_3 on the catalyst. Previous work shows that ammonium sulfate begin to decompose at 223 °C, but the H_2SO_4 that decomposes from ammonium sulfate still inhibits the SCR reaction under our experimental conditions [49].

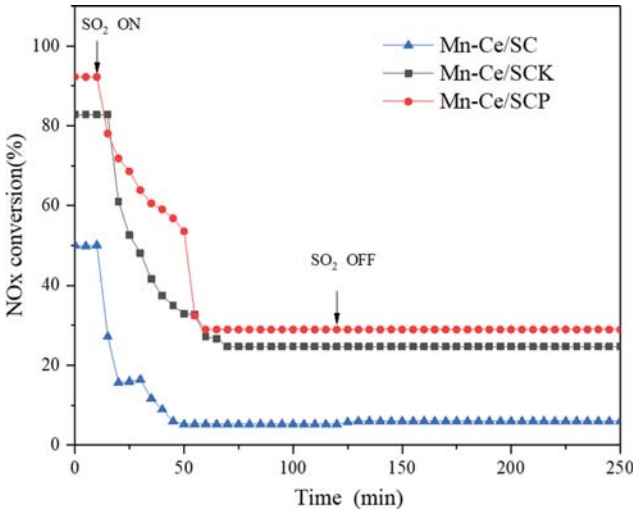

Fig. 13. SCR activity of three catalysts in the presence of SO_2 at 220 °C. Conditions: [NO]=400 ppm, [NH_3]=400 ppm, O_2=5% volume, SO_2=100 ppm, N_2 balance.

CONCLUSION

Sewage sludge char was used as low temperature catalyst support. To improve the deNOx activity of the catalyst based on sludge char, KOH and H_3PO_4 were used to activate it. KOH activation can highly increase specific surface area of SCK, which makes it have stronger adsorption capacity and more acidic sites, thus showing the best SCR catalytic performance. However, the catalyst activated by H_3PO_4 shows more oxygen-containing functional groups and unique phosphorus-containing oxygen functional groups, which makes the deNOx efficiency of the catalyst close to Mn-Ce/SCP. Both KOH and H_3PO_4 activation can increase the number of Brønsted acid sites. And the Brønsted acid sites are likely to be the main acid site of this type of catalyst for its adsorption and activation of NH_3. Moreover, sulfur poisoning on the SC surface at lower temperatures is irreversible. Hence, further studies on the improvement of SO_2 tolerance of SC based SCR catalyst are needed.

ACKNOWLEDGEMENTS

This work was supported by the Natural Science Foundation of Anhui province [1908085QE235], China Postdoctoral Science Foundation [2019M661688] and National Natural Science Foundation of China [Grant No. 51606001].

REFERENCES

1. A. Roger, *Atmos. Environ.*, **34**, 2063 (2000).
2. B. Zhu, S. Yin, Y. Sun, Z. Zhu and J. Li, *Environ. Sci. Pollut. Res.*, **24**, 24584 (2017).
3. Y. Wang, B. Shen, C. He, S. Yue and F. Wang, *Environ. Sci. Technol.*, **49**, 9355 (2015).
4. L. Lietti, I. Nova and P. Forzatti, *Top. Catal.*, **11**, 111 (2000).
5. L. Lietti, I. Nova, G. Ramis, L. Dall'Acqua, G. Busca, E. Giamello, P. Forzatti and F. Bregani, *J. Catal.*, **187**, 419 (1999).
6. S. Yang, C. Liu, H. Chang, L. Ma, Z. Qu, N. Yan, C. Wang and J.

Li, *Ind. Eng. Chem. Res*., **52**, 5601 (2013).
7. K. Kamasamudram, N. W. Currier, X. Chen and A. Yezerets, *Catal. Today*, **151**, 212 (2010).
8. Y. Yu, J. Zhang, C. Chen, C. He, J. Miao, H. Li and J. Chen, *J. Environ. Sci.-China*, **91**, 237 (2020).
9. X. Tang, J. Li, L. Sun and J. Hao, *Appl. Catal. B: Environ.*, **99**, 156 (2010).
10. X. Tang, J. Hao, H. Yi and J. Li, *Catal. Today*, **126**, 406 (2007).
11. Z. Wu, B. Jiang, Y. Liu, W. Zhao and B. Guan, *J. Hazard. Mater.*, **145**, 488 (2007).
12. Z. Fan, J. Shi, C. Niu, B. Wang, C. He and Y. Cheng, *Chem. Eng. J.*, **398**, 125572 (2020).
13. Z. Chen, Q. Yang, H. Li, X. Li, L. Wang and T. Chi, *J. Catal*., **276**, 56 (2010).
14. J. Pasel, P. Käßner, B. Montanari, M. Gazzano, A. Vaccari, W. Makowski, T. Lojewski, R. Dziembaj and H. Papp, *Appl. Catal. B: Environ.*, **18**, 199 (1998).
15. M. Kang, E. D. Park, J. M. Kim and J. E. Yie, *Appl. Catal. A: Gen.*, **327**, 261 (2007).
16. B. Jiang, Y. Liu and Z. Wu, *J. Hazard. Mater*., **162**, 1249 (2009).
17. J. Xie, D. Fang, F. He, J. Chen, Z. Fu and X. *Chen, Catal. Commun*., **28**, 77 (2012).
18. R. Jin, Y. Liu, Z. Wu, H. Wang and T. Gu, *Catal. Today*, **153**, 84 (2010).
19. W. S. Kijlstra, M. Biervliet, E. K. Poels and A. Bliek, *Appl., Catal. B: Environ*., **16**, 327 (1998).
20. Z. Wu, R. Jin, H. Wang and Y. Liu, *Catal. Commun*, **10**, 935 (2009).
21. R. Jin, Y. Liu, Y. Wang, W. Cen, Z. Wu, H. Wang and X. Weng, *Appl. Catal. B: Environ.*, **148-149**, 582 (2014).
22. L. Wang, Y. Zhang, J. Xu, W. Diao, S. Karakalos, B. Liu, X. Song, W. Wu, T. He and D. Ding, *Appl. Catal. B: Environ.*, **256**, 117816 (2019).
23. X. Wang, S. Wu, W. Zou, S. Yu, K. Gui and L. Dong, *Chin. J. Catal*., **37**, 1314 (2016).
24. Z. Zhu, H. Niu, Z. Liu and S. Liu, *J. Catal*., **195**, 268 (2000).
25. L. Zhu, B. Huang, W. Wang, Z. Wei and D. Ye, *Catal. Commun*., **12**, 394 (2011).
26. Y. Zhang, Y. Zheng, X. Wang and X. Lu, *Catal. Commun*., **62**, 57 (2015).
27. H. Yi, Z. Wang, H. Liu, X. Tang, D. Ma, S. Zhao, B. Zhang, F. Gao and Y. Zuo, *J. Chem. Eng. Data*, **59**, 1556 (2014).
28. B. Shen, J. Chen, S. Yue and G. Li, *Fuel*, **156**, 47 (2015).
29. J. S. Cha, J. Choi, J. H. Ko, Y. Park, S. H. Park, K. Jeong, S. Kim and J. Jeon, *Chem. Eng. J*., **156**, 321 (2010).
30. Y. B. Jo, J. S. Cha, J. H. Ko, M. C. Shin, S. H. Park, J. Jeon, S. Kim and Y. Park, *Korean J. Chem. Eng*., **28**, 106 (2011).
31. B. Shen, J. Chen, S. Yue and G. Li, *Fuel*, **156**, 47 (2015).
32. S. Singh, M. A. Nahil, X. Sun, C. Wu, J. Chen, B. Shen and P. T. Williams, *Fuel*, **105**, 585 (2013).
33. M. Si, Z. F. Wang, W. Ji, G. Yang, L. S. Liu, J. X. Wu, E. Y. Wang and X. Gou, *Appl. Mech. Mater.*, **694**, 484 (2014).
34. W. Li, S. Tan, Y. Shi and S. Li, *Fuel*, **160**, 35 (2015).
35. M. Kobayashi, R. Kuma, S. Masaki and N. Sugishima, *Appl. Catal. B: Environ.*, **60**, 173 (2005).
36. C. Liu, L. Chen, J. Li, L. Ma, H. Arandiyan, Y. Du, J. Xu and J. Hao, *Environ. Sci. Technol*., **46**, 6182 (2012).
37. Z. Liu, Y. Yi, S. Zhang, T. Zhu, J. Zhu and J. Wang, *Catal. Today*, **216**, 76 (2013).
38. Q. Shi, J. Zhang, C. Zhang, C. Li, B. Zhang, W. Hu, J. Xu and R. Zhao, *J. Environ. Sci. (China)*, **22**, 91 (2010).
39. T. Ge, B. Zhu, Y. Sun, W. Song, Q. Fang and Y. Zhong, *Environ. Sci. Pollut. Res*., **26**, 33067 (2019).
40. B. Buczek, S. Biniak and A. Świątkowski, *Fuel*, **78**, 1443 (1999).
41. R. Jin, Y. Liu, Z. Wu, H. Wang and T. Gu, *Chemosphere*, **78**, 1160 (2010).
42. C. F. Wu, M. A. Nahil, X. Sun, S. Singh, J. H. Chen, B. X. Shen and P. T. Williams, *J. Energy Inst*., **85**, 236 (2012).
43. D. A. Peña, B. S. Uphade, E. P. Reddy and P. G. Smirniotis, *J. Phys. Chem. B*, **108**, 9927 (2004).
44. F. Eigenmann, M. Maciejewski and A. Baiker, *Appl. Catal. B: Environ*., **62**, 311 (2006).
45. X. Wang, R. Duan, W. Liu, D. Wang, B. Wang, Y. Xu, C. Niu and J. Shi, *Appl. Surf. Sci*., **510**, 145517 (2020).
46. C. Gao, B. Xiao, J. Shi, C. He, B. Wang, D. Ma, Y. Cheng and C. Niu, *J. Catal*., **380**, 55 (2019).
47. T. Boningari, P. R. Ettireddy, A. Somogyvari, Y. Liu, A. Vorontsov, C. A. McDonald and P. G. Smirniotis, *J. Catal*., **325**, 145 (2015).
48. Z. Wu, R. Jin, Y. Liu and H. Wang, *Catal. Commun*., **9**, 2217 (2008).
49. P. Li, Q. Liu and Z. Liu, *Chem. Eng. J*., **181-182**, 169 (2012).